Transactions, SMiRT-24
BEXCO, Busan, Korea - August 20-25, 2017
Division II

INVESTIGATION INTO RESIDUAL STRESS EFFECTS ON APPARENT CLEAVAGE FRACTURE TOUGHNESS OF HIGH, MEDIUM AND VERY LOW CONSTRAINT GEOMETRIES

Jack Beswick[1], Prof Andrey Jivkov[3], Dr Peter James [4] and Prof Andrew Sherry[4]

[1]EngD Research Engineer, Nuclear Engineering, The University of Manchester/Amec Foster Wheeler, England
[2]Senior Lecturer, The University of Manchester, England
[3]Senior Consultant, Amec Foster Wheeler, England
[4]Chief Scientist, National Nuclear Laboratory, England

ABSTRACT

Non heat-treated welds in reactor pressure vessel structures are subjected to residual stress fields from welding, and the ferritic steels within the structures are susceptible to embrittlement from neutron irradiation, increasing the probability of cleavage fracture. This paper presents results from an on-going project to better understand and quantify the effects of constraint on cleavage fracture in such steels under various initial stress and strain conditions. The conditions investigated simulate non heat-treated welds in reactor pressure vessel structures. Previous work (Mahmoudi et al., 2008) has demonstrated that a residual stress field introduced through a double side punching method ahead of a crack serves to reduce the constraint parameter Q for high constraint geometries, but increase Q for low constraint geometries (Beswick, et al., 2015) (Hurlston et al., 2011). Such results, in conjunction with experimental failure data, have been used to postulate a failure curve in J-Q space (where J is the usual crack driving force), which could be used as a two-parameter fracture toughness in defect tolerance assessments. What was not previously considered was whether this failure curve extended into a region for very shallow cracks (i.e. very low Q) under similar initial conditions.

This paper includes findings from experiments that consider such very low constraint geometries. Specifically, fracture toughness tests were carried out on three-point bend specimens with normalised crack depths of a/W=0.4, 0.2 and 0.05. Initially, experiments were performed to reproduce the previous tests on higher constraint geometries without residual stress (Hurlston et al., 2011) for control and validation purposes. Following this, tests were conducted with and without the introduction of a similar residual stress field on the very low constraint geometries. The test results are presented in J-Q space and the paper includes comments on the applicability of a two-parameter fracture toughness curve that could be used under these initial conditions, and highlights the points requiring further experimental and theoretical investigation.

INTRODUCTION

Nuclear reactor pressure vessels (RPVs) are typically constructed from a ferritic steel clad with austenitic stainless steel. All of the major forged components comprising the RPV are joined through a welding process. Welding introduces residual stresses to the structure. A residual stress is one that is present despite there being no external load on the structure, typically caused by shrinkage mis-match during cooling of the steel, alongside phase changes which occur during the heating involved in the welding process. During construction of the RPV it is possible to relax residual stresses in several welds through post-weld heat treatment (PWHT). This process is, however, not possible for all welds within the structure, specifically transition welds between the RPV nozzles and the primary pipework, so significant residual stresses remain in the installed RPV.

Residual stresses have been shown to have significant effects on the effective cleavage fracture toughness of ferritic RPV steels (James et al., 2011). Cleavage fracture is a catastrophic mode of failure initiated by the breaking of second phase particles such as carbides in the presence of a macroscopic stress-concentrating defect. The breaking of the particle nucleates a microcrack which propagates into neighbouring grains of the ferrite matrix. If the fracture toughness of the ferrite is too low the crack propagation will not be arrested through plastification and macroscopic brittle fracture will occur, with some initial placticity (Kroon and Faleskog, 2005). This type of failure is usually associated with low temperatures and is therefore usually is not a concern during normal plant operation. The probablity of cleavage fracture is however increased through the increase in the ductile to brittle temperature observed after the long term neutron irradiaiton of RPV materials (Margolin et al., 1999). This combined with the lower temperatures experienced during routine plant shut downs make cleavage fracture a necessary consideration in structural integrity safety cases.

Structural integrity assessments will usually consider a single parameter to quantify the cleavage fracture toughness of the material in question. This property is measured through loading a cracked specimen, e.g. a Single-Edge-Notched-Bend (SENB) specimen (see Figure 1) to failure at a temperature that will ensure a cleavage mode of fracture. The load and crack-mouth opening displacement are measured and converted to a value of rack driving force J at failure using standardised equations, which is the fracture toughness. The test specimens have standardised designs with typical crack depth to wall thickness ratios of a/W=0.45-0.70 (ASTM, 2005). Specimens with these crack depths are considered high constraint geometries, where the plastic zone ahead of the crack is small in relation to the specimen dimensions. This is known as small scale yielding (SSY).

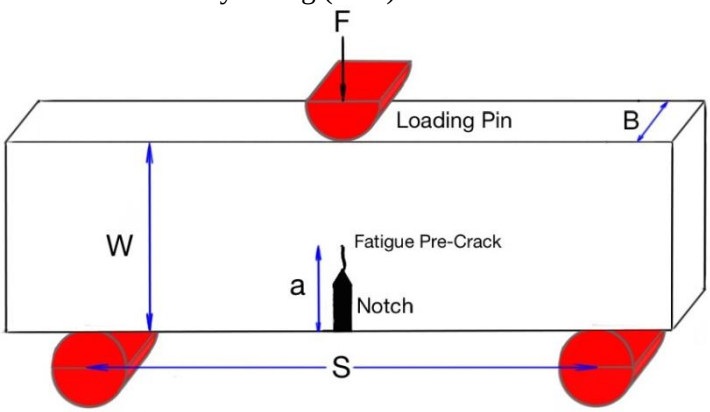

Figure 1. Schematic of SENB fracture toughness test

The high constraint fracture toughness calculated from these tests is then applied to real-world cracks and defects where handbook solutions or finite element analysis (FEA) are used to determine the limiting conditions (load and critical crack size) at failure of the structure what remaining lifetime could be expected. This high constraint fracture toughness approach is inherently conservative. The depth of the crack affects the growth of the plastic zone as well as the crack driving force (which is quantified by J). Typically, shorter cracks will have a larger plastic zone that reduces crack tip constraint and increases the apparent fracture toughness. This constraint effect is quantified through comparison of an idealised SSY stress field with that of the lower constraint geometry. This difference in stress field is quantified by the ‘Q’ parameter, which is a measure therefore of constraint. Q decreases through an increase in crack driving force and is therefore usually plotted against J. Hurlston et al. (2011) demonstrated that mechanically introduced residual stresses also have an effect on the Q parameter. Following cleavage fracture toughness testing of specimens with differing geometries and residual stress fields it was possible to populate the J-Q space with failure data, and a failure locus was postulated. This paper examines the viability of using such a failure locus in a wider range of structural assessments by extending the J-Q space into a region considering very low constraint geometries (very shallow cracks).

EXPERIMENTAL METHODS

Mahmoudi et al. (2008) and Hurlston et al. (2011) demonstrated that it was possible to introduce a residual, crack opening stress field, comparable to one that a defect in a welded structure may be subjected to, could be introduced through out of plane compression ahead of the crack. Numerical and experimental test results on SENB specimens were presented in these papers and it was shown that the closest simulation of an RPV weld residual stress field could be achieved through indenting the front and back surfaces equally with a double set of punches. A schematic of the double side punching method is shown in Figure 2. Deeper cracked specimens (a/W=0.42 and 0.42) had previously been tested (Hurlston et al. 2011) so it was decided that only very shallow cracked (a/W=0.05) specimens would undergo double side punching for the work presented in this paper.

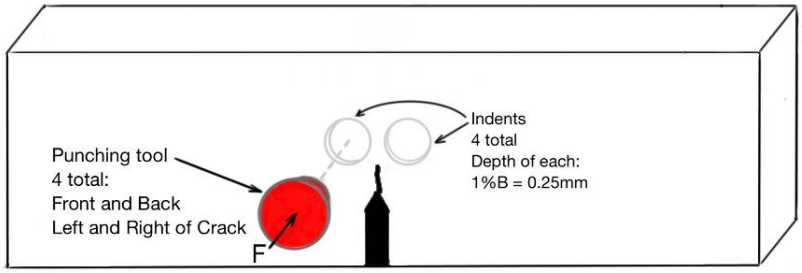

Figure 2. Double-side-punching schematic

The punches were positioned the same relative distance from the tip of the pre-crack as in Hurlston et al.'s (2011) experiments. In that test programme neutron diffraction was carried alongside predictions of the residual stress fields from finite element analyses, with sufficient agreement shown between the two that the stress fields from the FEA were validated for use in subsequent J-Q calculations. Similar FEA was carried out to test whether, despite the changes in crack and notch geometry, the residual stress fields would be similar for the very low constraint geometries. It was also necessary to assess whether carrying out the side punching after the introduction of a fatigue pre-crack as opposed to before would have a significant effect on the final residual stress field the crack was subjected to during the fracture toughness tests. The results of the FEA are presented in Figure 3.

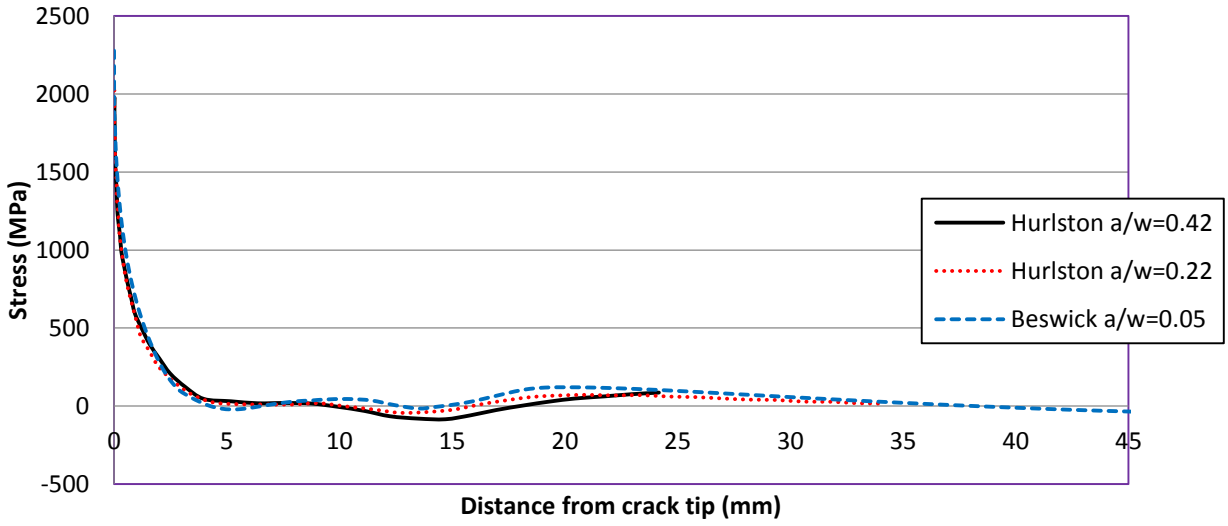

Figure 3. FEA crack opening residual stress fields at mid plane of specimen after pre-cracking

The agreement between the analyses was sufficient to suggest that a similar residual stress field would be introduced to the a/W=0.05 specimens and those previously tested such that any J-Q analyses could be compared with those in Hurlston et al.'s (2011) work, and it could be said a similar residual stress field had been present. Fracture toughness tests were carried out on SENB specimens, as per ASTM 1921 (ASTM, 2005), shown schematically in Figure 1. Their dimensions were W=50mm, B=25mm, S=200mm. 3 nominal crack depths were chosen: 20mm, 10mm and 2.5mm, to give a/W ratios of 0.4, 0.2 and 0.05 respectively. The former 2 crack depths were chosen for control purposes with the latter being used as the very low constraint geometries. For the a/W=0.4, 0.2 geometries, notches were machined into the specimens with integral knife edges included as shown in Figure 4, to allow a clip gauge to be attached. These required 2.5 mm of fatigue pre-cracks to be included to achieve the 'a' values desired. For the a/W=0.05 geometry specimens, only the leftmost 5mm (see Figure 4) of the notch was included in the initial specimen machining. This was added as extra material to the specimen blank, such that W=55mm. A fatigue pre-crack of 2.5mm was grown, and then the 5mm including the notch was skimmed away leaving the final a/W ratio of 0.05 (only pre-crack remaining), with W=50mm.

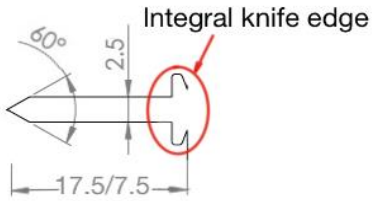

Figure 4. Notch geometry (dimensions in mm) for a/W=0.4, 0.2 specimens. a/W=0.05 specimens contained only leftmost 5mm of notch, and had no integral knife edges

The fracture toughness tests were carried out such that the load was increased through displacing the loading pin into the top of the specimen at a rate of 0.5mm/min, until fracture occurred. The tests were carried out at -140°C to ensure a cleavage mode of failure in all specimens and to again allow comparison with Hurlston et al.'s (2011) data (that test programme was also carried out at this temperature). A clip gauge was attached to the specimens such that the crack mouth opening displacement (CMOD) could be measured, along with the load from the actuator. It was not possible to include integral knife edges in the a/W=0.05 specimens so the clip gauge in these cases were attached to knife edges screwed into tapped holes at a distance of 2mm either side of the crack. A photograph of the experimental setup including the clip gauge is shown in Figure 5.

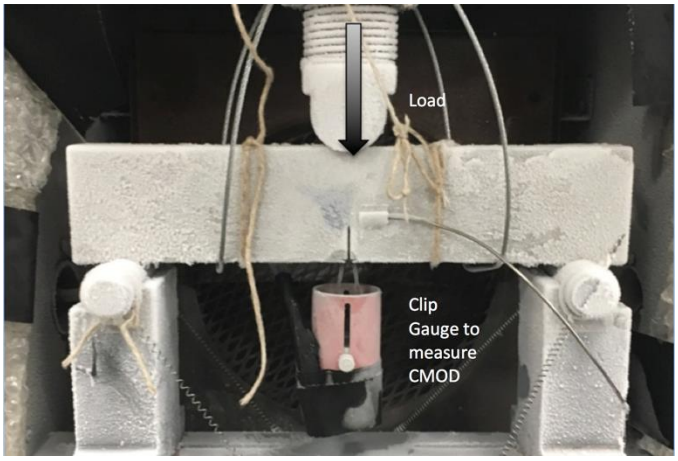

Figure 5. Photograph of fracture toughness test setup

FINITE ELEMENT ANALYSIS OF EXPERIMENTS

It was necessary to have an accurate and detailed description of the crack tip stress fields to enable J-Q analyses to be carried out. This was achieved through simulating the experimental procedure as realistically as possible using the commercial finite element software Abaqus™ (Dassault Systemes, 2013). The geometry of the equipment and specimens was recreated as close to reality as was feasible, including the side punches, loading pin and rollers. Some assumptions were however made including symmetry along the longitudinal and transverse central planes (such that a quarter model was created) of the specimens and straight crack fronts. Small strain assumptions were made to enable J calculations directly from the software, a sharp crack was also assumed for the same reason. The models were to be validated against the readings from the clip gauge. As these were fitted remote from the specimen in the low constraint specimen the knife edge was included in the model for these simulations. 3D linear 8 node hexahedral stress elements were used to mesh specimen model. The mesh was refined near the crack tip in concentric rings, the smallest elements being 2μm long. The crack tip elements were collapsible wedges to enable singularity calculations. The punches, loading pin and rollers were treated as analytical rigid bodies. Figure 1 and Figure 2 show schematics of the experimental set-ups which were recreated in the simulations.

The load was applied through contact between the specimen and loading pin which was displaced vertically into the specimen as with the experiments. The rollers on which the specimen sat were fixed throughout, contact between these and the specimen was also simulated for accuracy. The side punching process was also simulated as contact. Frictionless contact was assumed in all cases. To simulate the side punching it was necessary to constrain the top edge of the specimen in the vertical direction to prevent rigid body motion. This boundary condition was removed for the loading step. In the experiments, the side punching was carried out at ambient temperature, it was therefore necessary to have two sets of material properties, the ambient values (20°C) and those at which the fracture toughness tests were carried out (140°C). These material properties were input as Young's Moduli, and stress/plastic strain curves at the two temperatures. The data for these were extracted from historical tensile tests carried out on the material (A533b Class1). Ramberg-Osgood curve fits were applied to the tensile data remove some of the Luder's effect demonstrated in the material whilst remaining parallel to the work hardening slope; and allow strains to be estimated at the very high crack tip stresses. The tensile properties (up to 20% strain, full data extended to 1000%) used are shown in Figure 6.

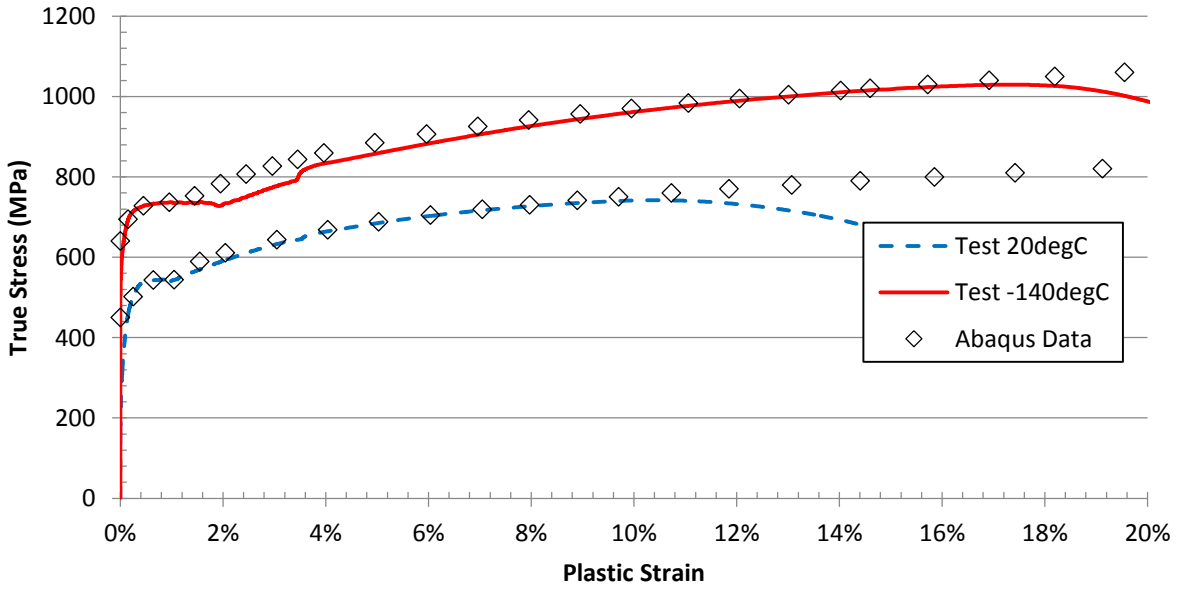

Figure 6. Tensile stress/plastic strain curves for A553b and material properties used in FE simulations

The simulations of the fracture toughness tests were validated against the load and clip gauge opening displacement (CGOD) data recorded during testing. In the case of the a/W=0.4, 0.2 tests, the clip gauge was attached directly to the integral knife edges so CGOD=CMOD. In the case of the a/W=0.05 specimens the clip gauges were remote from the specimen, so it was necessary to validate the simulations against the actual CGOD at the representative knife edge built in to the specimen model. These simulations offered the largest scope for discrepancy with the test data because they had the smallest CMODs, therefore this example is included in Figure 7 (Top) to demonstrate the validity of the models. Equally good agreement (within 5%) was shown with the a/W=0.4 and 0.2 specimens.

EXPERIMENTAL RESULTS

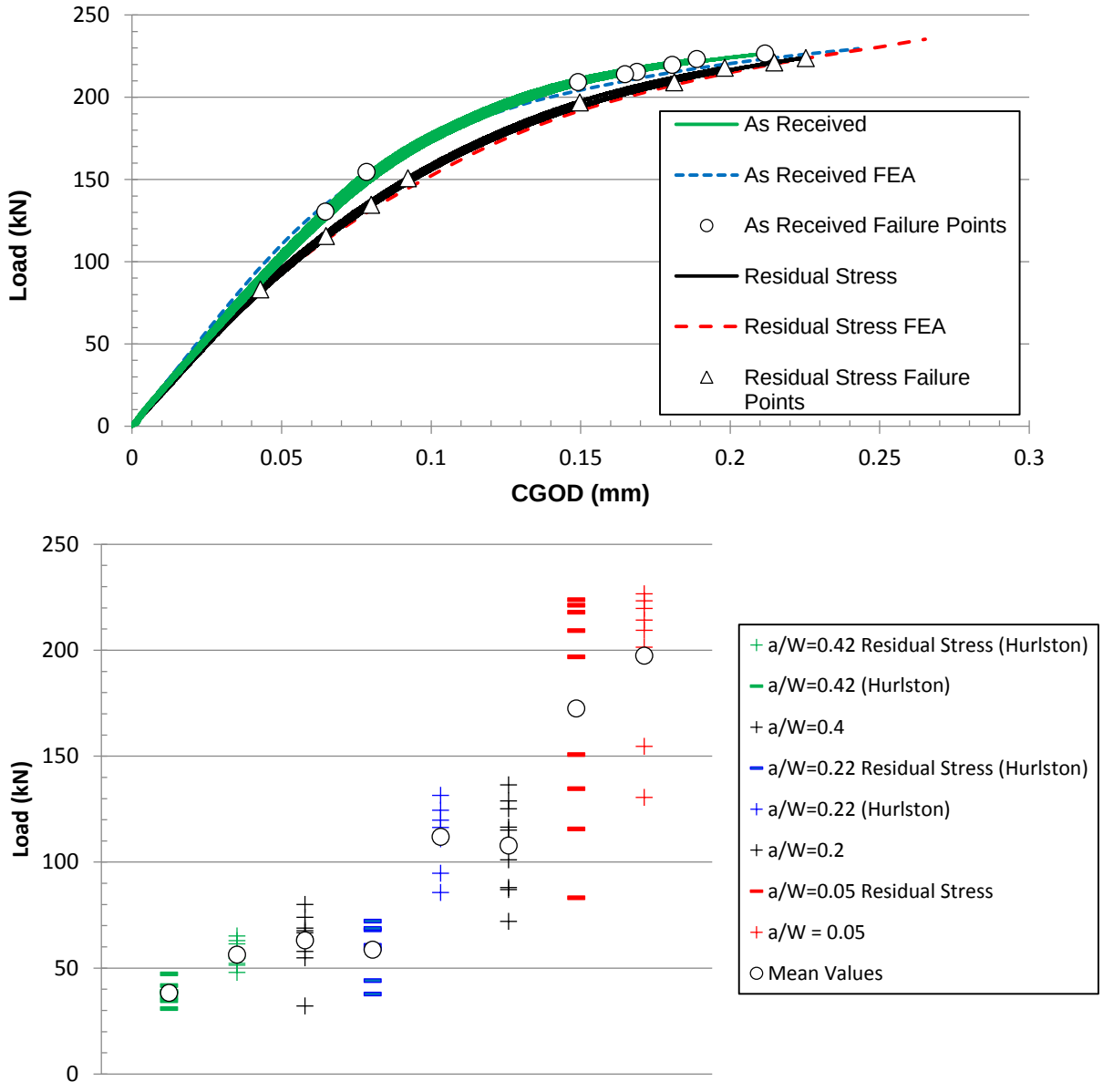

Figure 7. (Top) Load CGOD curves from FEA and experiments including failure points for very low constraint geometries (a/W=0.05)
(Bottom) Failure loads from all tests including those from previous project (Hurlston et al., 2011)

Figure 7 (Bottom) shows the failure loads for all of the tests under consideration in this paper. There are also included the load/CGOD curves for the a/W=0.05 specimens (Figure 7 (Top)). As has been described earlier the agreement between the FE simulations of the model and the test data demonstrates the validity of the modelling approaches taken. This is especially important in the case of the specimens with residual stress; the simulations following similar load CGOD traces in these cases show the side-punching and cooling processes have been accurately represented, allowing the inference that the stress fields within the models are suitably accurate to be used in the J-Q analysis. What can also be seen in Figure 7 (Bottom) is the comparison between the control tests (a/W=0.4, 0.2) and those from the previous project. Slightly higher scatter can be observed in the control tests than Hurlston et al.'s (2011) results for similar geometries. This is likely because of the fact that there is simply a larger sample size (10 tests as opposed to 7 in each case). The mean values for the high constraint tests show a 9% reduction between a/W=0.4 and 0.42, demonstrating a more significant geometrical effect than with the higher constraint tests (4% increase between 0.2 and 0.22). There were also changes in the manufacturing processes (length of fatigue pre-crack etc.) that could account for these differences, but as the averages remained within 10% it was decided that the two test programmes could be compared.

Table 1: Percentage reduction in failure load with residual stress

a/W	Lowest	Mean	Highest
0.42	35.6%	31.9%	27.5%
0.22	48.6%	47.6%	45.1%
0.05	36.3%	12.6%	1.2%

Table 1 outlines the reduction in failure load with residual stress for the highest, mean, and lowest values from the test programmes. This raises several points for consideration. Firstly it can be seen that the most consistent reduction in failure load is in the medium constraint geometry. This could be considered unusual because one may expect the residual stress to have the most significant effect to failure load in one extreme of geometry (deepest or most shallow cracks). What was observed by Hurlston et al. (2011), however, and can be seen in Figure 8 is that there appears to be a geometrical condition where there is a switch between the residual stress field increasing and decreasing constraint. This may go some way to explaining this observation: in the deep cracked geometries the reduction in constraint applied by the residual stress field is lessening the effect on failure load slightly when compared to the a/W=0.22 scenario, where the constraint is increased, providing a more detrimental effect.

This however is then disputed by the very shallow cracked geometries. In these cases the reduction in the lowest failure load with the introduction of residual stress is significant and similar to that of the a/W=0.42 tests. However the scatter of the tests shows that these specimens did not fail consistently at lower loads, in fact a large proportion of the tests failed at the same higher loads as the as received material, increasing the mean and highest failure loads. This suggests that in the very low constraint geometries residual stress may be completely washed out through loading, having little effect on the fracture behaviour in some cases, although as it cannot be said this happens in all occurrences, any engineering assessment considering these results must consider the lower bound failure probabilities.

POSTULATED J-Q TRAJECTORIES AND IMPLICATIONS TO FAILURE LOCI

The Q parameter, first postulated by O'Dowd and Shih (1991) is a higher order term in the description of crack tip stresses, expanding the Williams functions used in simple elastic-plastic fracture mechanics. The value of Q represents the difference in stress between a finite geometry and that within an idealised SSY situation (where the plastic zone size r_p<0.2 x other major dimensions). The SSY field can be generated using a boundary layer model (BLM) which simulates a semi-infinite crack in an infinite

body. For the results presented in this paper, a semi-circular mesh was used (symmetry exploited), with a radius of 1m. The model was meshed using 2D linear 4 node plane strain elements, again refined at the crack tip to 2μm, and again small strain assumptions were made. The material properties used were the same as the test simulations at -140°C. The model was loaded to a prescribed value of J by using the Westergaard functions to calculate the necessary displacement at its circumference.

Following the boundary layer simulation, the crack opening stresses (σ_{11}) were extracted along the ligament (symmetry line) of the model. These stresses (normalised by the material's yield stress: σ_0) were plotted against the normalised distance from the crack tip ($r\sigma_0/J$, where r is the distance from the crack tip). Curves of this nature were extracted for each increment of loading. For the boundary layer model this provided a set of self-similar curves which collapse onto each other essentially leaving a single curve representing the SSY field. A similar process was carried out for each increment of loading of the fracture toughness test simulations. This produced a set of approximately parallel curves which are not self-similar. The difference in normalised stress field between the SSY and finite geometry simulations at a distance $r\sigma_0/J=2$ is the Q parameter, and was plotted against the crack driving force, J at each increment of loading. This analysis gave a set of trajectories which allowed quantification of crack-tip constraint through loading of the specimen. These are presented for the high and medium constraint geometries in Figure 8, with the J-Q curves from Hurlston's work extracted directly from Hurlston et al. (2011), to demonstrate the variation between their analyses and those carried out for this test programme. Included also are the failure points, where J was calculated using FEA, at the central plane of the ligament, as opposed to applying standards such as ASTM 1921 (ASTM, 2005) to the experimental data , to allow comparison with Hurlston et al's (2011) data, who also used the FEA J values.

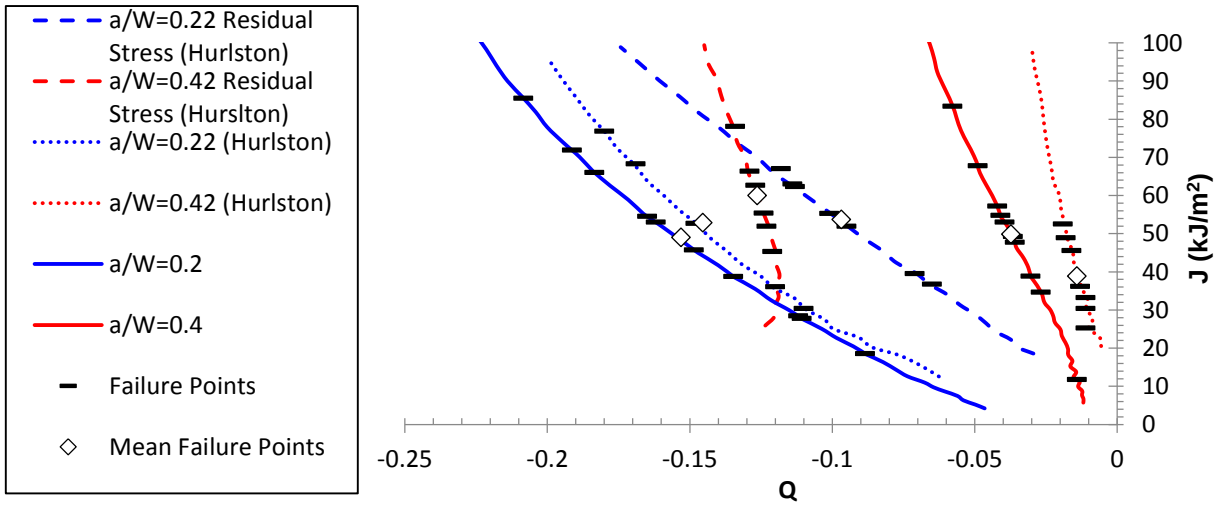

Figure 8. J-Q failure points from high and medium constraint geometries (Hurlston et al. 2011)

Several things were observed from these plots. As can be seen there is a general tendency for the values of J values at failure (J_c) to increase as Q decreases, demonstrating the viability of 2 parameter fracture toughness. The reduction in constraint is attributed to larger plastic zones in these geometries which increases the apparent fracture toughness. It can be seen that the slight geometric differences in the test specimens (a/W=0.2, 0.4 as opposed to 0.22, 0.42) has not only a more significant effect on failure load (as shown in Figure 7 (Bottom)) at high constraint, but also on the J-Q trajectory; there is a more noticeable shift in the trajectory between the a/W=0.42 and 0.4 curves than the a/W=0.22 and 0.2. As has been commented on in the previous section there is also an interesting shift between the residual stress field decreasing Q for the high constraint tests but reducing it at lower constraint. This is attributed to the fact that the introduction of the hydrostatic stresses caused by the side punching (designed to simulate the welding process) serve to increase triaxiality (and therefore constraint) in the a/W=0.22 specimens, but actually reduce it in the higher constraint geometries because there is a more significant contribution from

the opening mode dominated residual stress field in this geometry (Hurlston et al. 2011). When considering the values in Table 1, this appears to be corroborated by the experimental findings, in that the failure load seems to be reduced more with residual stress in the medium constraint geometries. More difficult to explain is the higher mean values of J_c in the specimens with residual stress. As was shown in Figure 7 (Bottom), the mean failure loads were lower in all geometries with residual stress; therefore, an accurate representation of the testing should mirror this.

Consideration was given to the method of calculating J for use in the a/W=0.05 trajectories to enable residual stress to be considered in the analysis. Path independent J values were calculated from the a/W=0.05 simulations including residual stress using the JMOD method described in Lei et al. (2000) that allows the initial strain field (ε_{ij}^0) under residual stress to be treated as a constant during subsequent deformation, where the applied mechanical strain (ε_{ij}^m) increases under the applied stress from loading (Equation 1), which is incorporated into Abaqus™ (Dassault Systemes, 2013):

$$w = \int_0^{\varepsilon_{ij}^m} \sigma_{ij} d\varepsilon_{ij}^m$$
$$J = \int_\Gamma \left(w dy - \sigma_i \frac{\partial u_i}{\partial x} \right) n_i \, ds + \int_A \left(\sigma_{ij} \frac{\partial \varepsilon_{ij}}{\partial x} \right) dA \quad (1)$$

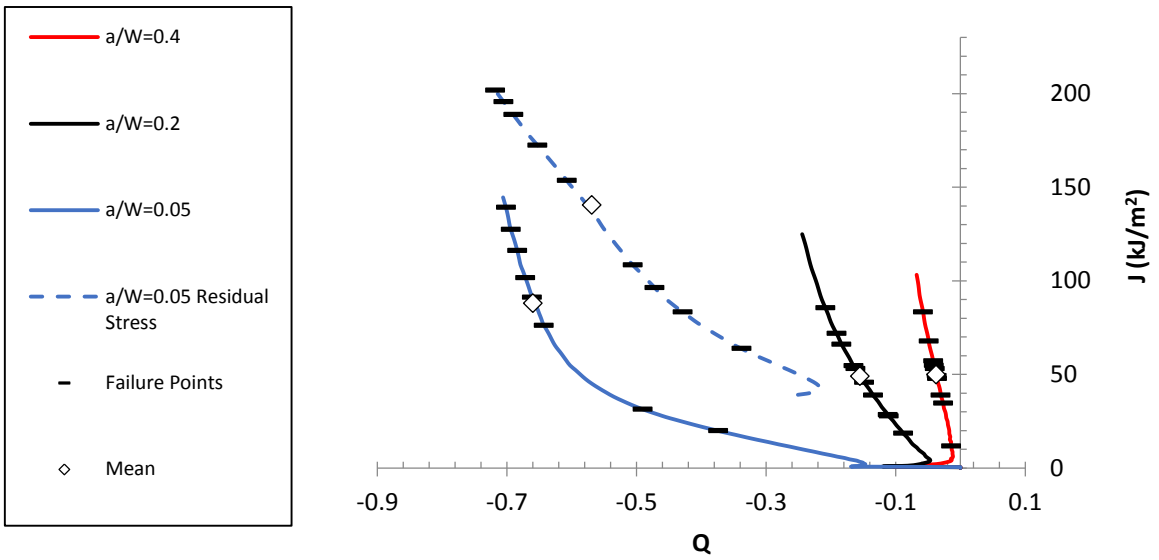

Figure 9. J-Q trajectories and failure points for high, medium and very low constraint geometries, with all results calculated directly from FEA, JMOD (Lei et al, 2000) used for J values involving residual stress

The output from the JMOD method (Lei et al. 2000) demonstrated that there was a crack driving force (J_{res}) present prior to any external loading being applied in the simulation. It is unclear if Hurlston et al. (2011) used this method or another to extract J values from their simulations but they are quoted as using the FEA results for to calculate J_c from the corresponding failure load (scoping calculations suggested JMOD or similar may have been used based on load/J agreement of similar simulations); and with or without the JMOD (Lei et al., 2000) method the FEA J values always included a J_{res} value, which would explain the unrepresentatively high J_c values when residual stress was included (see Figure 8). This effect was apparently much more significant in the a/W=0.05 specimens (J_{res}=31kJ/m^2) as can be seen in Figure 9. Again the significantly higher J_c values with residual stress demonstrated a misrepresentation of what occurred in reality. It was therefore decided to consider what effects zeroing J_{res} at the start of the loading step would have on the J-Q trajectories. This would not only effect the vertical J-based position of the loading curve, but Q also, as the normalised distance $r\sigma_0/J=2$ would be altered. Alongside this the

method of calculating J_c was altered. As opposed to extracting the J value at the failure load form the simulations, consideration was given to the J-values extracted from testing, specifically using ASTM 1921 (ASTM 2005), which allows a plasticity correction for shallow cracked specimens such as the ones under consideration here. When using the method in the standard to calculate J, the residual stress is essentially treated as zero as only the area under the load/displacement plots such as those in Figure 7 (top) contribute to the result. It was decided that these J values, when considered in conjunction with the path-independent J-Q loading curves calculated from the FEA, may provide a more accurate representation of the physical outcomes of the test programme. These results are shown in Figure 10.

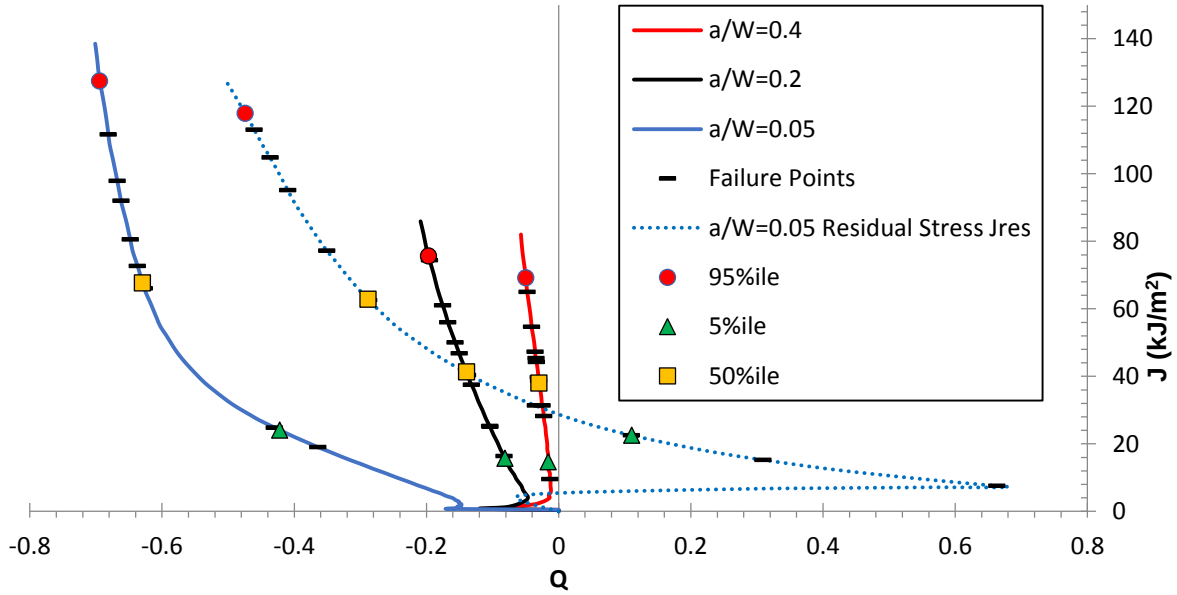

Figure 10. J-Q trajectories and failure points for high, medium and very low constraint geometries, J_{res} for residual stress trajectory zeroed, J_c values calculated using ASTM 1921 (ASTM 2005), failure probability percentiles from master curve (Wallin, 1984)

As can be seen taking this approach to presenting the test results provides a better description of what has physically happened in the testing. There can be see a reduction in all percentiles of failure probability (based on the master curve approach (Wallin, 1984)) when residual stress has been introduced to the a/W=0.05 specimens. There is however the greatest reduction in the higher percentiles, and barely any when considering the 5%ile failure probability (~2kJ/m^2), which is the opposite trend to the failure loads shown in Figure 7 (Bottom) and Table 1. The positive Q is deemed to be acceptable because in the early stages of loading the residual plus applied stress opening mode stress fields are larger than that of the applied SSY field under the same crack driving force. There is however increase in the 5%ile J, with Q in this positive region, when considering all of the test scenarios. This would go against a failure trend of a reducing J as Q increases. There is also only a very slight decrease in the median values of J for a significant increase in Q between in the a/W=0.05 scenarios with the introduction of residual stress. All of these observations suggest that the residual stress curve may be better positioned much closer to its as-received counterpart in the J-Q space (Q more negative). As the stress fields used in the calculations have been shown to be sufficiently validated the only remaining variable to be considered is the method of calculating J. Further exploration is required as considering both the JMOD (Lei et al., 2000) and ASTM 1921 (ASTM, 2005) methods have as yet not enabled a definitive failure curve to be drawn in the J-Q space when considering residual stress. It is possible that considering non-proportional stress increases in the calculations will provide a better representation of how J evolves under the applied load.

CONCLUDING REMARKS

This work has outlined the reasons why two-parameter fracture toughness may be suitable for certain defect tolerance assessments in the cleavage regime, and why cleavage fracture could specifically be a concern in nuclear plant. To better assess the viability of this constraint based fracture toughness, an experimental test programme was carried out including very low constraint geometries. These tests provided new insight into the fracture behaviour of ferritic steel in the cleavage regime, and the experimental methods have been detailed. Numerical simulations of the experiments have been carried out, allowing the Q parameter (which quantifies constraint) to be calculated. This Q parameter was plotted in terms of the crack driving force, J, for the tests both with and without a mechanically introduced residual stress field.

After plotting the failure data from the tests in this J-Q space it became apparent that the average failures for tests including residual stress could be higher than the J-Q calculations from the as-received material might suggest, if a constraint based fracture toughness is viable. Therefore the J values were altered such that the initial J due to the crack opening from the introduction of the residual stresses (J_{res}) was zeroed at the first increment of loading. The results from these calculations suggested that this an improvement in terms of the J-Q failure points representing the behaviour in the tests, although it has still not been possible to suggest a definitive failure curve for this material when considering residual stress. It is believed that the main reason for this is the method of calculating J under residual stress, in that neither the ASTM or JMOD approach seems to accurately represent the evolution of J through loading for this geometry where a residual stress field is present.

REFERENCES

ASTM. (2005). "E1921-05: Standard test method for determination of reference temperature, T0 , for ferritic steels in the transition range."

Beswick, J., Jivkov, A., James, P., and Sherry, A. (2015). "Investigation of a two parameter approcah to assessments of defects in residual stress fields," *SMIRT 23,* Manchester, England

Dassault Systemes. (2013). "Abaqus Standard 6.13."

Hurlston, R., Sharples, J. K., and Sherry, A. H. (2011). "Investigation into the effect of Residual Stress on Crack-Tip Constraint and Brittle Fracture," *ASME Conference on Pressure Vessels and Piping.* Baltimore, Maryland.

James, P., Hutchinson, P., and Madew, C. (2011). "Provisional Results for an Experimental Investigation into the Effect of Combined Primary and Secondary Stresses When Considering the Approaches of R6 and the recently Developed g() Factor." *ASME Conference on Pressure Vessels and Piping.* Baltimore, Maryland.

Kroon, M., and Faleskog, J. (2005) "Micromechanics of cleavage fracture initiation in ferritic steels by carbide cracking." *Journal of the Mechanics and Physics of Solids* 53, 1, 171-196.

Lei, Y., O'Dowd, N. P. and Webster, G. A. (2000). "Fracture Mechanics Analysis of a Crack in a Residual Stress Field." *International Journal of Fracture*, 106, 195-216.

Mahmoudi, A. H., Truman C. E., and Smith D. J. (2008). "Using Local Out-of-Plane Compression (LOPC) to Study the Effects of Residual Stress on Apparent Fracture Toughness." *Engineering Fracture Mechanics*, 75, 1516-1534.

Margolin, B. Z., Shvetsova V. A., and Gulenko A. G. (1999). "Radiation embrittlement modelling for reactor pressure vessel steels: I. Brittle fracture toughness prediction." *International Journal of Pressure Vessels and Piping*, 76, 715-729.

O'Dowd, N. P., and Shih C. F. (1991). "Family of Crack-Tip Fields Characterized by a Triaxiality Parameter--I. Structure of Fields." *Journal of the Mechanics and Physics and Solids,* 39, 8, 989-1015.

Wallin, K. (1984). "The Scatter in KIC results." *Engineering Fracture Mechanics*, 19, 1085-1093.